# Passive impedance spectroscopy of EV Lithium-ion batteries in transient operation

Jules MILLET[1], Daniel DEPERNET[1], Ali SARI[2], Frédéric GUSTIN[3], and Hugo HELBLING[2]

[1]Université Marie et Louis Pasteur, UTBM, CNRS, Institut FEMTO-ST, F-90000 Belfort, France
[2]Université Claude Bernard Lyon 1, Ampère, UMR5005, INSA Lyon, Ecole Centrale de Lyon, CNRS, Villeurbanne, F-69100, France
[3]Université Marie et Louis Pasteur, CNRS, Institut FEMTO-ST, F-90000 Belfort, France

**Abstract**

Impedance characterization of a Lithium-ion cell is a commonly used method to assess its state of health or internal temperature. However, Electrochemical Impedance Spectroscopy (EIS) requires a dedicated excitation system and can only be performed under steady-state conditions, making it challenging to implement onboard. The objective of this work is to develop a passive EIS method, which does not require an external excitation device and allows impedance estimation even under dynamic operating conditions. This paper proposes an impedance measurement approach based on the analysis of the naturally occurring harmonic content in electric vehicle driving cycles. To achieve this, a signal processing algorithm was developed to extract and analyze these harmonics while compensating for non-stationary effects related to current, State of Charge (SoC), and temperature. The methodology is validated through experimental tests reproducing realistic operating conditions.

*Keywords:* EIS, Battery, Passive impedance measurement, Signal processing, Driving cycle

**Graphical abstract**

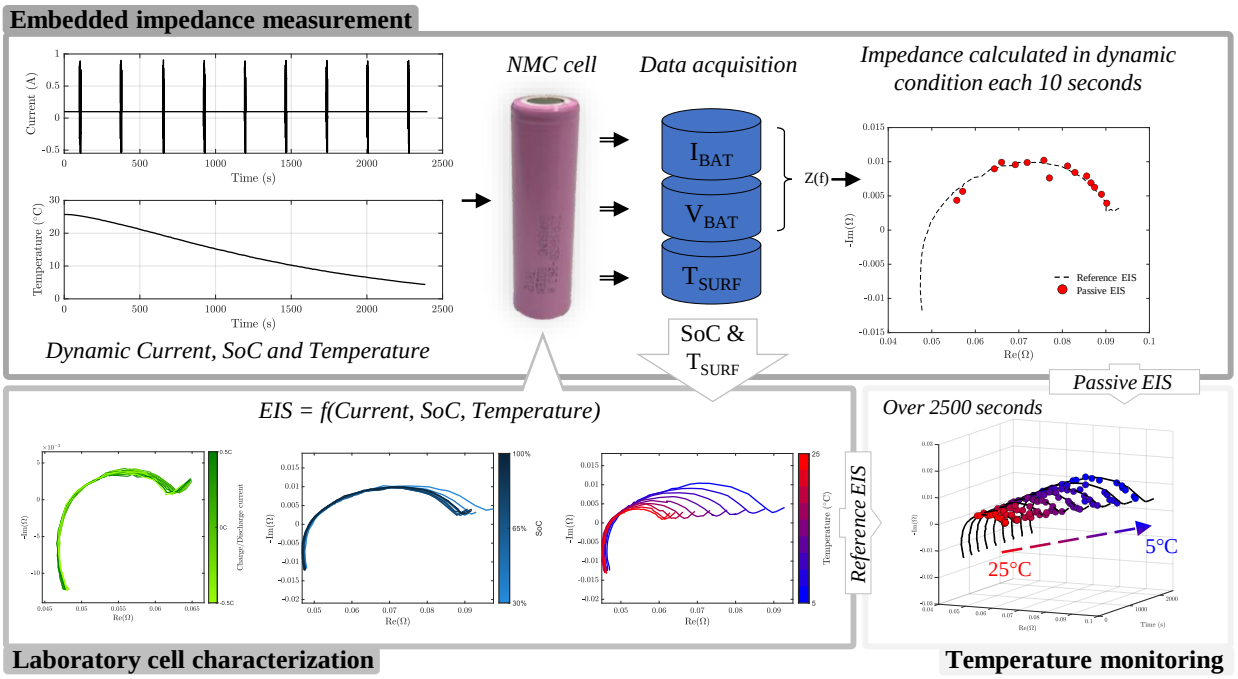


# 1 Introduction

In the context of the energy transition, reducing the environmental impact of the transportation sector is a major challenge [1]. The electrification of vehicles, through electric vehicles (EVs), is seen as a key strategy to address this issue. However, large-scale deployment of EVs raises several challenges, particularly regarding the lifecycle management (manufacturing, usage, recycling, and repurposing) of Lithium-ion (Li-ion) batteries, which are the core component of the propulsion system [2]. Indeed, the degradation of these batteries directly affects vehicle range, performance, and safety, and indirectly influences their environmental footprint.

In light of these challenges, increasing attention is being paid not only to the optimization of battery usage during their first life, but also to their repurposing in stationary applications, paving the way for a second life. This approach extends the service life of batteries while contributing to material recyclability, provided that their State of Health (SoH) can be accurately assessed.

Ensuring a reliable and real-time diagnosis of battery SoH is therefore essential. Among the available methods [3, 4], electrical impedance analysis, and particularly EIS, stands out for its ability to identify internal electrochemical processes across a wide frequency range. This technique is now widely recognized as a reference for characterizing aging mechanisms [5, 6] and enhancing internal temperature monitoring [7, 8].

However, the application of EIS in embedded contexts remains complex. Generating an excitation signal requires specific technical means, and maintaining the battery in a steady-state condition during EIS can impact vehicle availability. Indeed, several studies have proposed using the power converter as a signal generator [9, 10, 11], notably through duty cycle modulation. However, this approach is restrictive and highly dependent on the vehicle's electronic architecture.

A promising avenue involves leveraging naturally occurring signals during driving cycles, without the need for artificially injected signals. Several studies have demonstrated the potential of this strategy [12, 13, 14], particularly through frequency analyses and impedance calculations using optimized signal processing algorithms. However, these approaches still face two major limitations: the difficulty of identifying relevant frequencies within a complex signal, and the non-stationary behavior of the battery due to dynamic driving conditions. The latter is especially critical [15], as it directly affects the quality of the impedance estimates.

This article specifically addresses this issue. It presents a passive impedance estimation method designed to exploit the natural harmonics generated by the powertrain while accounting for non-stationary phenomena. This approach enables impedance estimation under realistic battery usage conditions during vehicle operation, without disrupting normal operation or requiring specific hardware modifications.

In this context, the first part of the article provides an analysis of the parameters affecting non-stationarity and their impact on electrochemical impedance. Then, an original signal processing method is introduced, leveraging the natural harmonics generated during driving cycles to passively estimate impedance. Finally, the approach is experimentally validated through a series of studies, including test bench experiments, electrochemical cell characterization, and impedance tracking under dynamic conditions.

# 2 Parameters Influencing Non-Stationarity and Their Effects on Electrochemical Impedance

Electrochemical Impedance Spectroscopy is a widely used tool for studying internal electrochemical phenomena [16]. This technique is based on applying a sinusoidal excitation signal at a given frequency and at a fixed operating point, allowing the analysis of the voltage and current responses. By repeating this process over a wide frequency range, it is possible to obtain the impedance spectrum of the battery.

Its use is particularly relevant when the system is under stationary conditions, that is, when the parameters that influence impedance remain stable, such as temperature, SoC,

SoH, or current. This stationarity condition is a standard requirement to ensure the validity and reproducibility of impedance measurements [15].

However, this requirement becomes a limitation when studying systems subjected to dynamic conditions, as is the case in this study [15]. Temporal variations in SoC, temperature, or current complicate the direct interpretation of impedance spectra. Therefore, as a first step, it is necessary to investigate the evolution of impedance under various stationary conditions. This will help better interpret the responses observed under non-stationary conditions.

To gain a deeper understanding of the underlying phenomena, it is essential to associate the various contributions of the impedance spectrum with internal electrochemical processes, and more specifically with Equivalent Circuit Models (ECMs) [17]. This association provides a more direct interpretation of the physical components and chemical effects reflected in the results (Figure 1).

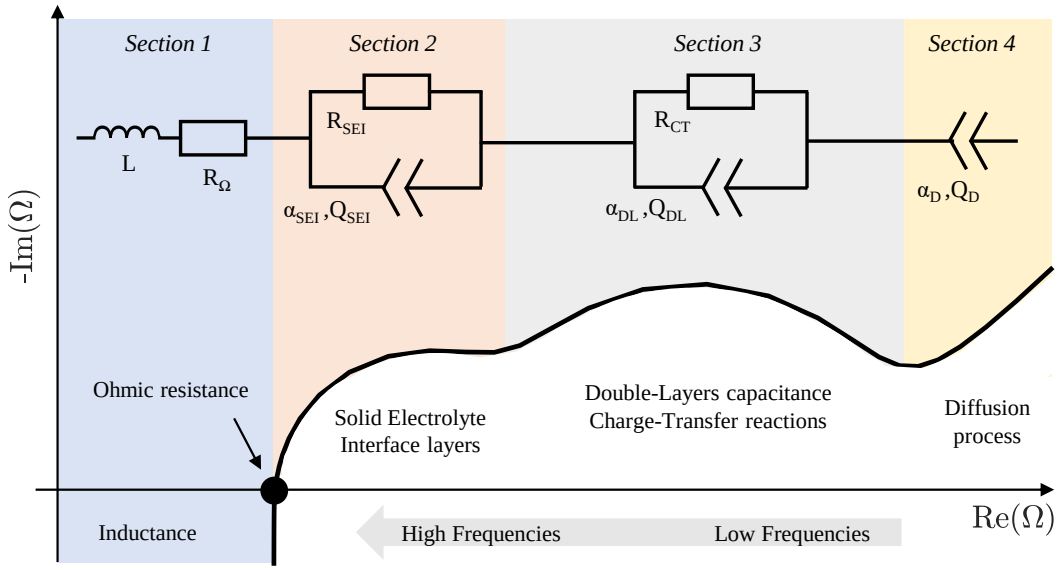


Figure 1: Nyquist diagram from EIS with the corresponding Equivalent Circuit Model

Extensively studied in the literature [16, 18], the impedance spectrum can generally be divided into four main regions (Figure 1):

- Section 1: At very high frequencies, inductive effects from metallic components appear, followed by the ohmic resistance ($R_\Omega$), which reflects the intrinsic resistances of the cell's materials and interfaces.
- Section 2: Solid Electrolyte Interphase (SEI) response: associated with capacitive and resistive phenomena at the electrode–electrolyte interface.

- Section 3: Charge transfer process and double-layer capacitance: reflects the kinetics of electrochemical reactions at the interfaces.
- Section 4: Diffusion (Warburg region, low-frequency): associated with ionic diffusion processes within the electrodes.

Numerous studies have highlighted how these different impedance contributions evolve depending on the operating conditions (current, SoC, temperature, SoH) [6, 19]. The study by J. Li et al. [20] analyzes the sensitivity of the EIS spectrum to various influencing variables and specifies, for each condition, which sections of the impedance are impacted:

- Current: slightly affects the charge transfer resistance;
- State of Charge : mainly affects the charge transfer resistance and diffusion processes;
- Temperature: influences both the SEI resistance and the charge transfer resistance;
- State of Health : impacts the ohmic resistance, charge transfer resistance, and diffusion behavior.

Based on these observations, a sensitivity ranking has been established, from the most to the least influential factor: SoH > temperature > SoC > current. However, J. Li et al. [20] also point out that SoH and temperature have a more significant impact than SoC and current on certain impedance components [14]. These results highlight the value of impedance monitoring as a diagnostic tool, particularly for tracking internal temperature and the state of health of the battery.

Moreover, these parameters also influence the stationarity of the system during EIS measurements [21]. It is essential to consider the time constant associated with each parameter, since an EIS measurement typically lasts several minutes [9]. As a result, not all parameters challenge the stationarity condition to the same extent.

For instance, current has a very short time constant (nearly instantaneous response), making it particularly critical under dynamic conditions. SoC and temperature evolve over intermediate time scales and can also induce non-stationary effects during the measurement. In contrast, SoH, which is characterized by a very long time constant (evolving over the long term), can be considered quasi-stationary over the duration of an EIS measurement.

Therefore, in the context of our study, system non-stationarity is primarily attributed to variations in current, SoC, and temperature, while SoH is assumed to remain stationary during the measurement. These considerations define the dynamic conditions under which our system is studied.

It is now necessary to identify how impedance evolves under such dynamic conditions and to determine appropriate analysis methods capable of extracting meaningful information about the state of the batteries. The method was developed so that it can detect impedance variations regardless of the source of the change, whether it is current, SoC, temperature, or SoH.

# 3 Signal Processing Algorithm

The objective of this method is to achieve passive EIS, meaning without signal injection, under dynamic conditions. The first step is to identify the harmonics naturally present in the battery current. The second step involves studying algorithms and methods that can leverage these harmonics under dynamic conditions to compute the associated impedance. A synthesis of the research conducted has been presented, which then enables the proposal of an optimized signal processing algorithm. The choice of parameters for this processing is explained to ensure optimal accuracy in impedance estimation.

## 3.1 Origin of Current Harmonics in Electric Traction

The harmonics naturally present in embedded power electronics systems offer a unique opportunity for Passive EIS (PEIS). Indeed, the power converters used in the traction chain generate current harmonics on the DC bus [22, 23]. These harmonics are directly related to the inverter control laws, particularly Pulse Width Modulation (PWM). The choice of modulation type influences both the amplitude and the frequency of the harmonic components observed on the DC bus, as noted by B. P. McGrath [23].

Studies by B. P. McGrath et al. and J. Hu et al. indicate that these harmonics are unavoidable, even in well-designed systems, due to switching effects, transistor dead times, and mechanical nonlinearities [23, 24]. The resulting harmonic spectrum is relatively broad, extending from a few tens of hertz up to several kilohertz. In terms of amplitude, the dominant low-frequency DC-link current harmonics are typically several orders of magnitude lower than the phase fundamental current, with amplitudes on the order of $10^{-3}$ to $10^{-2}$ relative to the phase current, as can be estimated from the analytical spectra reported by McGrath et al. [23].

In conventional traction systems, the dominant low-frequency harmonic components are typically located at integer multiples of the motor fundamental frequency [23, 24]. Furthermore, as highlighted in the work of H. Hu et al. [24], in a motor/gearbox assembly, these motor-induced harmonics create periodic variations in currents and torques, resulting

in well-identified frequency signatures on the DC bus. During real driving conditions, additional frequency components originating from the driving profile further enrich the spectral content propagating through the converter to the battery.

The objective of this study is not to exactly reproduce specific harmonic frequencies or amplitudes, but rather to consider excitation frequencies and amplitudes within physically realistic ranges. In practice, the harmonic amplitudes present on the DC bus strongly depend on the inverter control strategy, operating point, load conditions, and DC-link sizing, which makes a precise a priori estimation difficult. Therefore, the experimental tests rely on representative harmonic frequencies and amplitude levels chosen to reflect realistic operating conditions, allowing the proposed method to be evaluated while accounting for variations in harmonic amplitude.

Analyzing this naturally occurring harmonic content, without introducing any additional excitation signal, enables passive impedance observation.

## 3.2 Exploitation of Harmonics

Several studies have investigated the estimation of a Li-ion cell impedance from driving cycles, without relying on specific excitation signals. In this context, a notable early contribution is that of Lohmann et al. [13], who analyzed the frequency content of a driving cycle. The Goertzel algorithm was employed [25], under the assumption that the frequencies of interest were already known. This work laid the foundation for the approach, although it was limited to cases where signal processing targets only pre-defined injected frequencies.

B. Liebhart et al. [12] further developed this approach by focusing on the estimation of Li-ion battery impedance from the dynamic regimes of a driving cycle, using power spectral density analysis. Through a signal processing method based on segmentation, they were mainly able to estimate impedance in the high-frequency range (100 Hz to 1 kHz).

More recently, B. Yang et al. [14] revisited part of this methodology, inspired by the PEIS technique developed by Liebhart et al. [12], and applied it to various types of driving cycles, urban, mountainous, and rural. The results are promising, as they demonstrate the feasibility of exploiting these signals without prior knowledge of their frequency content.

Analysis of this body of work highlights a critical need: the development of a robust signal processing algorithm capable of estimating impedance from natural harmonics under dynamic conditions. Existing approaches already provide some elements of a solution. Indeed, unlike excitation signals used in electrochemical impedance spectroscopy, signals derived from driving cycles exhibit harmonics with unknown frequencies and amplitudes. This implies that observation windows are not necessarily synchronized with the frequencies of interest, which necessitates the use of segmentation and windowing techniques.

However, these studies face several limitations. Notably, the issue of signal stationarity is not addressed, despite being a key factor in improving estimation accuracy. Under dynamic conditions, the stationarity assumption is generally invalid, leading to signal drift over time and compromising the quality of impedance estimation.

This specific challenge is precisely what the algorithm developed in this study aims to address, by explicitly accounting for non-stationary phenomena.

## 3.3 Detailed Algorithm

To address these specific challenges, a rigorous methodology has been developed to enable reliable impedance calculation under dynamic conditions. The proposed approach builds upon the previously discussed work, while introducing a key contribution: the compensation of signal drift through a dedicated correction procedure.

This method is designed to mitigate the effects induced by the non-stationary nature of the signals, which remains a major limitation in existing techniques. By integrating this compensation mechanism, the algorithm enhances the accuracy of impedance estimations derived from the natural harmonics present in driving cycles.

The following outlines the different stages of the proposed signal processing methodology, from the measured time-domain signals to the estimation of the cell impedance (Figure 2):

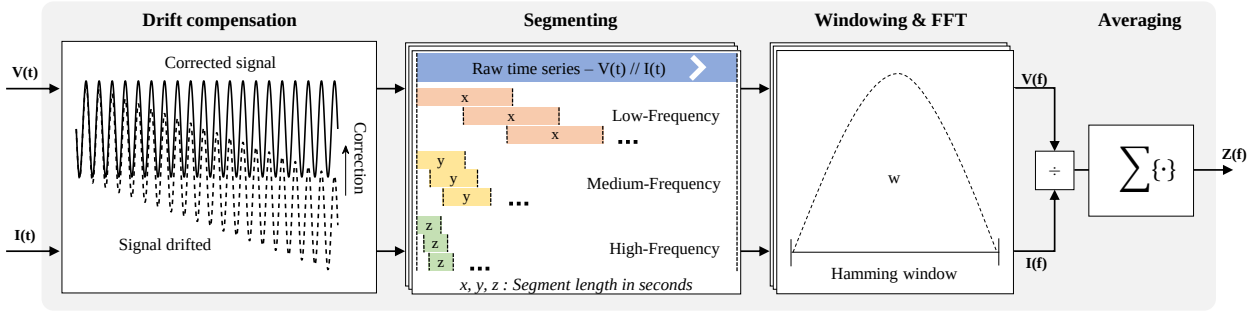


Figure 2: Optimized signal processing algorithm

**Drift Compensation**: During impedance measurement, any deviation from a stationary state can lead to a progressive voltage drift [15]. This drift, often caused by slow phenomena such as electrochemical polarization or thermal variations, distorts the low-frequency components of the signal. If not corrected after acquisition, it can bias the frequency-domain analysis and thus impair the accuracy of impedance estimation. Therefore, compensating for this drift is essential to ensure the reliability of the results. In addition to compensating for drift, the frequency ranges (segmentation) are separated so that only the frequencies of interest are kept in each range.

**Segmentation**: Segmentation consists in dividing the voltage and current signals into multiple segments of equal duration [26]. These durations are defined based on the three targeted frequency ranges: high, medium, and low frequencies. This segmentation enables observation of the entire frequency spectrum relevant to the battery's impedance by adapting the sampling frequency to the selected range. Moreover, the segments are not extracted sequentially without overlap; instead, they are generated with a defined overlap ratio to enhance frequency detection, as illustrated in Figure 2.

**Windowing & FFT**: A windowing function is then applied to limit spectral leakage and reduce discontinuities at the signal boundaries. Since the signals under analysis are dynamic, windows such as Hamming, Hanning, or Gaussian are used to attenuate edge effects [27], thereby improving the quality of the resulting spectrum. Following this, a Fast Fourier Transform (FFT) is applied to convert the signal from the time domain to the frequency domain.

**Averaging**: Averaging is used to smooth out random variations due to noise or signal variability. Additionally, impedance values are averaged for each detected frequency over a time window shorter than the thermal and state-of-charge time constants, in order to improve measurement reliability. This approach is particularly useful for monitoring impedance variations, for example by measuring over multiple windows during changes in temperature or state of charge. By following these steps, impedance estimation becomes feasible under dynamic conditions. Now that the algorithm has been described, it can be tuned, a key strength of this approach.

## 3.4 Selection of Parameters

In the proposed algorithm, two parameters have a significant impact on the impedance estimation: the cutoff frequency associated with drift compensation, and the selected frequency ranges under analysis.

### 3.4.1 Frequency Ranges

The frequency ranges are determined by a few key factors: the number of points per period required at the lowest and highest detectable frequencies in each band, the available computation time, and temperature effects. To maintain reliable impedance measurements, a minimum of 10 points per period is imposed. To prevent overly long computations, the number of points per period is capped at 100. Taking these constraints into account, and using equation (1), several distinct frequency ranges can be defined. [9].

$$F = \frac{F_s}{N_{pts} \cdot Dec} \tag{1}$$

Let $N_{\text{pts}}$ denote the minimum or maximum number of points required for the detected frequency in each range, $F_s$ the sampling frequency, $F$ the minimum or maximum frequency to be detected, and Dec the decimation factor.

However, it is essential to define the overall frequency range beforehand, in order to observe the desired electrochemical phenomena. Identifying which phenomena are detectable within a given frequency range is crucial. As discussed previously, ohmic behavior, SEI formation, and charge transfer processes are strongly influenced by temperature and the cell's SoH. These phenomena can be observed in the frequency domains corresponding to Sections 1, 2, and 3 of Figure 1 [28, 29], which typically span from the kilohertz range down to tenths of a hertz, depending on the cell chemistry and design. Based on the characteristics of the cells used in this study [8], the chosen working frequency range extends from 1 Hz to 1000 Hz. The decision was made to exclude the diffusion-related Warburg region (below 1 Hz), which is associated with drift from a stationary state. Three sub-frequency bands were defined as follows:

- A high-frequency band: 1000 Hz to 100 Hz;
- A mid-frequency band: 100 Hz to 10 Hz;
- A low-frequency band: 10 Hz to 1 Hz.

The voltage and current measurements, combined with appropriate decimation, allow for the required number of points per segment to be obtained. This, in turn, enables impedance calculation with sufficient resolution across the selected frequency bands.

### 3.4.2 Cutoff Frequency: Drift Filter

Drift compensation is achieved by applying a low-pass filter, whose purpose is to separate the slow variations due to stationary drift from the fast signals associated with EIS excitation. To do this, an appropriate cutoff frequency must be defined, allowing a clear distinction between the slow dynamics and the signals relevant for the measurements.The distinction is made through the impedance spectrum by identifying the frequency where the charge-transfer and diffusion parts intersect. This provides a spectrum rich in information when sweeping the frequencies, thanks to the non-stationary behavior.

A digital filter is used for this step. After comparing common options, the key factors were how the filter shapes the amplitude, the amount of ripple, how sharp the cutoff is, and

how it handles phase. The filter needed to stay as linear as possible in phase, which narrowed the choice to Bessel and Butterworth. Butterworth offered the best overall tradeoff, so it was selected. An eighth-order design was chosen to get fast attenuation.

In addition to compensating for the drift, for each of the three frequency ranges we analyzed, a specific cutoff frequency is set based on the minimum frequency of the corresponding range. This allows the ranges to be separated and only the frequencies of interest to be retained. In this way, the cutoff frequencies are designed both to separate the frequency bands and to compensate for the drift (Table 1). This compensation is applied to both voltage and current signals to prevent any amplitude or phase errors.

Table 1: Selected cut-off frequency

| **Name** | **Range Frequency** | **Cut-off Frequency** |
|---|---|---|
| High frequencies (HF) | 1000 to 100 Hz | $F_c = 75\,\text{Hz}$ |
| Medium frequencies (MF) | 100 to 10 Hz | $F_c = 7.5\,\text{Hz}$ |
| Low frequencies (LF) | 10 to 1 Hz | $F_c = 0.75\,\text{Hz}$ |

Each segment within each frequency range is thus rectified and corrected using the filter and by subtracting the filtered signal from the unfiltered one, with the goal of eliminating drift and offset. The choice of parameters is crucial to obtain accurate impedance measurements. This is precisely the strength of the algorithm, which allows these parameters to be adjusted in order to optimize measurement accuracy. The algorithm was first implemented and configured in MATLAB to validate its functionality, and then prepared for application to more practical cases.

# 4 Experimental Application

This section focuses on the experimental application of PEIS, based on the optimized signal processing algorithm. Three main steps are required for this approach: validating the developed algorithm, performing the electrochemical mapping of the tested cell, and analyzing its behavior during a representative driving cycle.

All measurements were carried out on a dedicated test bench, designed to characterize the cell under various experimental conditions such as temperature, SoC, and current. The tests were conducted on a cylindrical Samsung ICR18650-26J cell (NMC111 cathode), with a nominal voltage of 3.7 V and a nominal capacity of 2600 mAh.

## 4.1 Test Bench

An electronic load (Chroma), connected in parallel with an ITECH power supply, enables precise control of the current applied to the battery. The voltages and currents in the circuit are observed and measured using a Tektronix oscilloscope with 8-bit resolution. The current is measured with a clamp meter that provides ±2% accuracy. The voltage is measured with a sensor connected to a calibration circuit that amplifies it with a gain of 18. Combined with the oscilloscope's selected range, this setup ensures reliable measurements of both voltage and current. The entire setup is controlled via a LabVIEW interface, which ensures automatic recording of voltage, current, and temperature data.

The test bench (Figure 3), equipped with a thermal chamber, allows for cell testing under various temperature conditions. In addition to internal chamber temperature measurement, a surface temperature measurement system has been implemented. A PT100 sensor, connected in a four-wire configuration to a National Instruments board via a CompactDAQ system, enables accurate surface temperature measurements of the cell. Furthermore, open-circuit voltage (OCV) measurements combined with coulomb counting are used to estimate the SoC of the cell.

This test bench makes it possible to inject excitation signals under controlled operating conditions in order to establish reference EIS measurements. It also supports the injection of driving cycles to be used for passive EIS.

Two measurement methods are used depending on the type of EIS performed:

- Reference EIS: Voltage and current are measured for each frequency by taking 10,000 points per frequency. The sampling frequency and the voltage and current per division are adjusted accordingly to achieve the best possible precision and resolution. A file containing 10,000 points for voltage and current is generated for each frequency.

- Passive EIS: Voltage and current are measured over a duration that depends on the injected cycle. Unlike reference EIS, the sampling frequency is fixed. Additionally, a file containing all the points is generated, allowing the proposed signal processing method to be applied.

For this purpose, the bench was used to validate the signal processing algorithm.

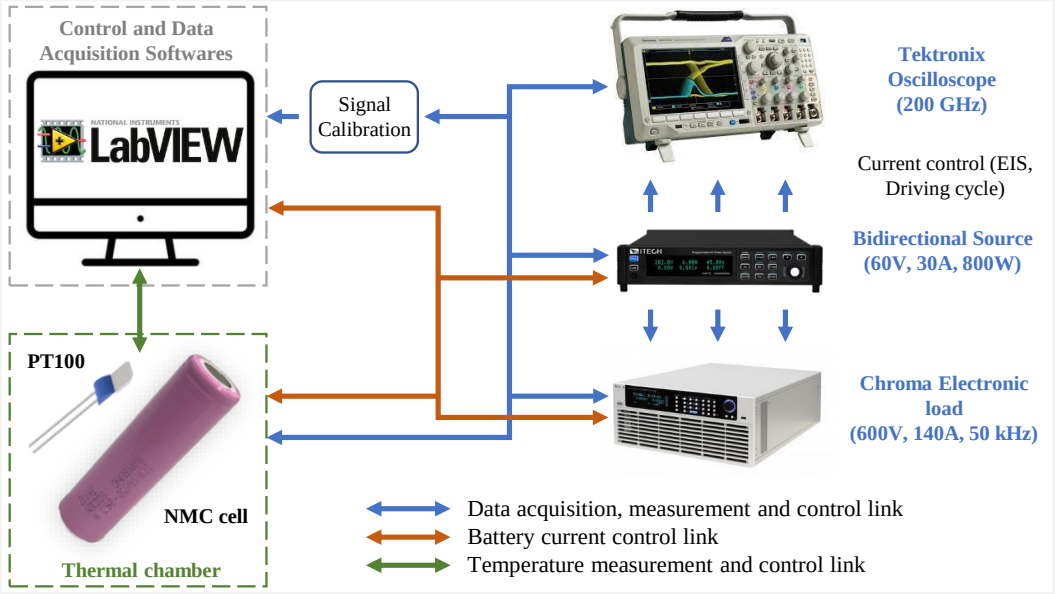


Figure 3: Experimental test bench designed for passive and reference EIS

## 4.2 Electrochemical Characterization of the Cell

Electrochemical characterization of the cell is a crucial step in understanding the factors influencing battery impedance under real operating conditions. To this end, EIS measurements are performed at various charge and discharge currents, different SoC levels, and under a range of temperatures.

A conventional signal processing algorithm, distinct from the one developed above, is used to establish these reference EIS datasets. It analyzes the signals at each injected frequency, adjusting the sampling frequency and acquisition window to obtain the optimal number of data points, thereby ensuring the highest possible impedance measurement accuracy [9].

Traditionally, cell characterization is conducted at zero current to minimize variations in temperature and state of charge. However, in this study, which focuses on the analysis of driving cycles involving a continuous current component, the characterizations are carried out at non-zero operating points. This approach also avoids rest periods, which are known to influence impedance measurements [30].

Accordingly, two measurement campaigns were conducted using the LabVIEW-based test bench supervision system to characterize the cell's behavior.

Table 2: EIS campaign at different currents

| # | Process | Units |
|---|---|---|
| 1 | Set the Temperature of the cell in the thermal Chamber | 2h Before test |
| 2 | Measure OCV, Calculate SoC | Instantaneous before Test |
| 3 | Cell preheating | 2 min at 0.25C and 2 min at -0.25C |
| 4 | 14 EIS test at $SoC_{initial} = 90\%$ | $I_{DC} = [\pm 0.1, \pm 0.3, \pm 0.5, \pm 0.7,$ |
| | EIS during discharging / charging | $\pm\, 0.9, \pm 1.1, \pm 1.3]$ A, |
| | No relaxation time | $I_{AC} = 0.25$ A, |
| | | $f_{inj} = 0.01$ Hz $-$ 10 kHz |
| 5 | Repeat the procedure for all Temperature | $T_{amb} = [5, 15, 25]°C$ |

A first measurement campaign aimed to evaluate the impact of current on impedance (Table 2). To this end, EIS measurements were performed at various operating points, both in charge and discharge, and at several temperatures, covering a frequency range from 10 kHz to 0.1 Hz.

Table 3: EIS campaign at different SoC levels and temperatures

| # | Process | Units |
|---|---|---|
| 1 | Set the Temperature of the cell in the thermal Chamber | 30 min Before test at 25°C |
| 2 | Measure OCV, Calculate SoC | Instantaneous before Test |
| 3 | Cell preheating | 2 min at 0.25C and 2 min at -0.25C |
| 4 | 1 EIS tests at $SoC_{initial} = 100\%$ | $I_{DC} = 0.5$ A, $I_{AC} = 0.5$ A, |
| | EIS during discharging | $f_{inj} = 0.01$ Hz $-$ 10 kHz |
| | No relaxation time | |
| 5 | Discharge cell by 8% of $SoC_{initial}$ | 0.75 A, 0.3C for 900 s |
| 6 | 1 EIS test ($SoC_{initial}$ – 8%) | $I_{DC} = 0.5$ A, $I_{AC} = 0.25$ A, |
| | EIS during discharging | $f_{inj} = 0.01 - 10$ kHz |
| | No relaxation time | |
| 7 | Repeat (steps 5, 6 until SoC drops to 30%) | |
| 8 | Repeat the procedure for all Temperature | $T_{amb} = [5, 15, 25]°C$ |

A second campaign was then conducted to assess the impact of the cell's SoC on impedance (Table 3). EIS measurements were performed every 15 minutes under a constant discharge current of 0.2 C, at three different temperatures. This methodology allows for characterization of the impedance evolution as a function of SoC, from 100% down to 30%, without any rest periods between steps, thereby avoiding transient effects associated with relaxation [30].

The obtained spectra (Figure 4.a) show a very slight variation in impedance [19] as a function of current. This variation can be attributed to the combined effects of current on charge transfer and the internal Joule heating it induces [31, 32]. These results indicate that the influence of current on impedance is minor compared to that of temperature, SoC, and SoH [6, 33]. However, the self-heating associated with increased current must be taken into account. To this end, the surface temperature measurement described earlier provides a more accurate estimation of the cell's internal temperature. Given the temperature variations observed during EIS measurements under varying current, impedance changes are primarily attributed to Joule heating, while the influence of current on charge transfer is considered

negligible in this study for the tested cell.

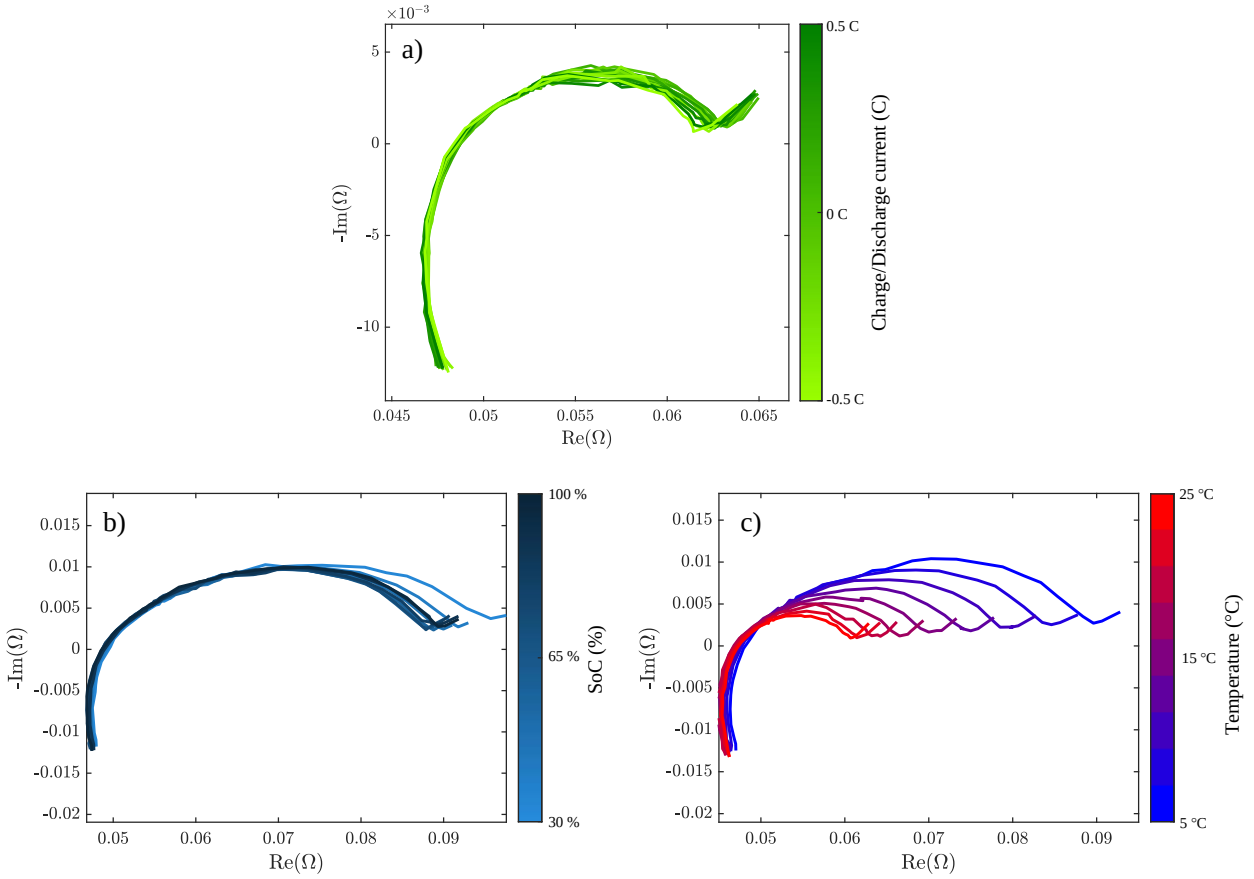


Figure 4: (a) Reference EIS measurements as a function of current at 25°C and 90% SoC, (b) State of Charge at 0.2C and 5°C , (c) Temperature at 0.2C and 90% SoC

The analysis of spectra as a function of SoC (Figure 4.b) also shows impedance variations at low frequencies, mainly due to changes in electrochemical kinetics. Kinetics are generally less favorable at both low and high SoC, leading to an increase in charge transfer resistance in these regions. This phenomenon occurs at both low and high temperatures.

Regarding the spectra as a function of temperature (Figure 4.c), they clearly show that impedance is highly temperature-dependent. At low temperatures, impedance increases significantly, particularly with respect to the charge transfer resistance and the resistance associated with the SEI layer. This is due to slower electrochemical reactions and reduced ionic conductivity. These observations highlight the significant impact of temperature on the electrochemical behavior of the cell.

This characterization campaign provides insight into the influence of current, SoC, and temperature on impedance. Furthermore, the mapping is validated by the literature discussed in Section 2, given the similarity of the results. The data obtained will serve as a reference

for comparisons with data collected under real operating conditions, particularly during the analysis of the driving cycle. The next step, following the algorithm validation, will consist of identifying the frequency components of the driving cycle and their associated impedances.

## 4.3 Validation of the Drift Compensation Method

To validate the drift compensation method, an EIS measurement was performed under conditions that induce significant drift. Specifically, the EIS was conducted at a current of 2A, a temperature of 25°C, and a SoC of approximately 90%, which leads to a voltage drift due to the applied current. The resulting spectrum was processed in two ways: first, using a signal processing algorithm without drift compensation, and second, using the algorithm with drift compensation.

To assess whether the processed signal is valid, the Kramers-Kronig (KK) method was applied [34]. This method evaluates the stationarity of a signal by analyzing its linearity. Specifically, the Kramers-Kronig relations are used to estimate the real part of the impedance from its imaginary part, and vice versa (2)(3).

$$Z_{\mathrm{Re}}(\omega) = \frac{2}{\pi} \int_0^{\infty} \frac{\omega' \, Z_{\mathrm{Im}}(\omega')}{\omega^2 - \omega'^2} \, d\omega' \tag{2}$$

$$Z_{\mathrm{Im}}(\omega) = -\frac{2}{\pi} \int_0^{\infty} \frac{\omega' \, Z_{\mathrm{Re}}(\omega')}{\omega^2 - \omega'^2} \, d\omega' \tag{3}$$

More specifically, this method allows for assessing the linearity of the analyzed signal from the impedance spectrum by estimating the residual at each frequency (4)(5).

$$\Delta_{\mathrm{Re}}(\omega) = \frac{Z_{\mathrm{Re}}(\omega) - \hat{Z}_{\mathrm{Re}}(\omega)}{|Z(\omega)|} \tag{4}$$

$$\Delta_{\mathrm{Im}}(\omega) = \frac{Z_{\mathrm{Im}}(\omega) - \hat{Z}_{\mathrm{Im}}(\omega)}{|Z(\omega)|} \tag{5}$$

As a general rule, minimum and maximum thresholds are defined for the residual, allowing determination of whether the signal can be considered linear. This threshold is typically set at 0.5%, beyond which the system is no longer considered linear [35].

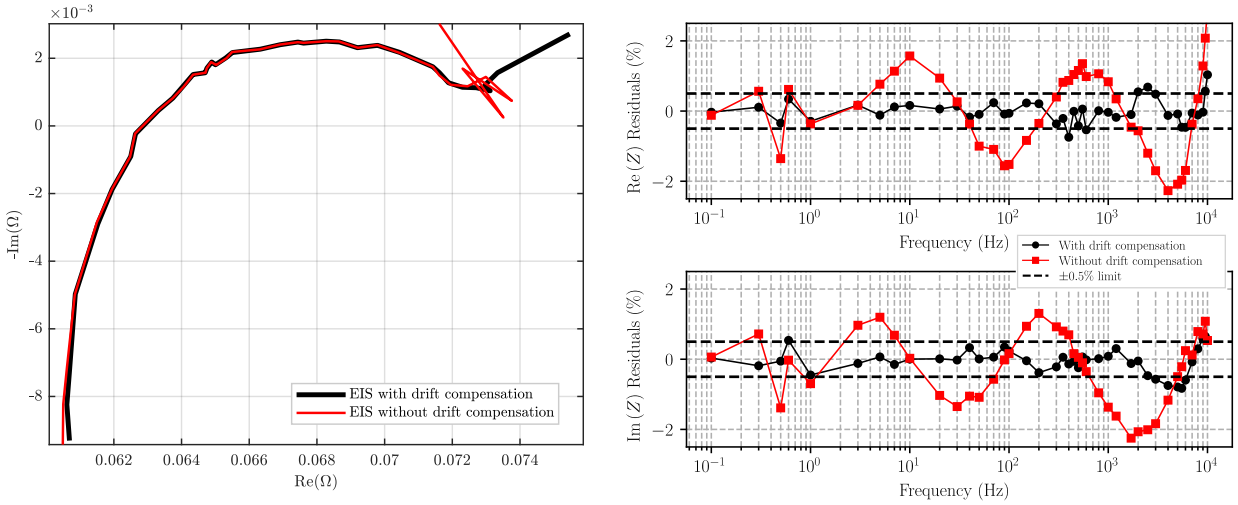


Figure 5: EIS performed with and without drift compensation and corresponding residuals analysis

The spectra in Figure 5 clearly demonstrate the importance of drift compensation, especially at low frequencies. Furthermore, residual analysis highlights non-linearity, with residuals exceeding the 0.5% threshold. It should be noted, however, that in both cases, inductive effects related to the test setup slightly affect signal linearity. This effect is nonetheless considered negligible in our analysis, as this part of the spectrum is not under study.

The next objective is to test the optimized algorithm with drift compensation by comparing it to a conventional signal processing algorithm.

## 4.4 Validation of the Algorithm on a Spectrum

This approach aims to test the optimized algorithm on the same signal obtained under steady-state conditions by comparing the impedance spectrum it produces with that derived from a conventional signal processing algorithm (used for the reference EIS).

The conventional algorithm analyzes the signals at each injected frequency by adjusting the sampling frequency and acquisition window to obtain the optimal number of points, thereby ensuring the highest possible accuracy in impedance measurement. This method establishes the reference EIS.

In contrast, the optimized algorithm analyzes the same signal acquired at a fixed sampling frequency, reflecting embedded system conditions. It then employs decimation, segmentation, and overlapping techniques, presented in the previous section, to exploit a maximum number of time windows and effectively detect the frequencies present in the signal. This corresponds to passive EIS.

Both EIS measurements were performed consecutively while maintaining the battery under steady-state conditions. The reference EIS takes 3 minutes and 30 seconds for a full frequency range (0.1 Hz to 10 kHz), with the processing algorithm analyzing one acquisition file per injected frequency, and 1 minute and 10 seconds for a reference EIS over the reduced frequency range used for the passive EIS (1 Hz to 1 kHz). In contrast, the passive EIS lasts 10 seconds and uses the optimized algorithm, which processes a single file containing all injected frequencies.

Table 4: Reference EIS vs Passive EIS

| **Process** | **Reference EIS** | **Passive EIS** |
|---|---|---|
| Current | 0.5A | 0.5A |
| Sinus injection | 0.1 Hz to 10 kHz | 1 Hz to 1 kHz |
| Sampling frequency | 250 Hz to 25 MHz | 10 kHz |
| Windowing | One | Hamming |
| Knowledge of injected frequencies | Yes | No |
| EIS duration | 3 min 30 | 10 seconds |
| Outside temperature | 5°C | 5°C |
| SoC | $\approx 90\%$ | $\approx 90\%$ |
| Signal processing algorithm | Conventional | Optimized |

Thus, the differences presented in Table 4 allow distinguishing between the reference EIS and the passive EIS.

In this approach, the passive EIS is tested and compared with the reference spectra to validate the signal-processing algorithm. The steps of the method are shown from the current and voltage measurements up to the impedance calculation for each frequency range. First, the current and voltage signals are recorded (Figure 6.a). Drift compensation and frequency-band separation are then carried out with filters to perform the segmentation of the signals for each range (Figure 6.b). Each segment is windowed, and a FFT is applied to extract the spectral components. The impedance is computed from the frequency content of each windowed segment, which then makes it possible to average the impedance over the selected period, here 10 seconds. Figure 6.c shows the spectra obtained by both methods: the reference EIS is displayed in black, and the passive EIS in red. The detected frequency ranges appear on the spectrum, showing that PEIS can capture both high and low frequencies. The identified frequencies are listed in Table 5.

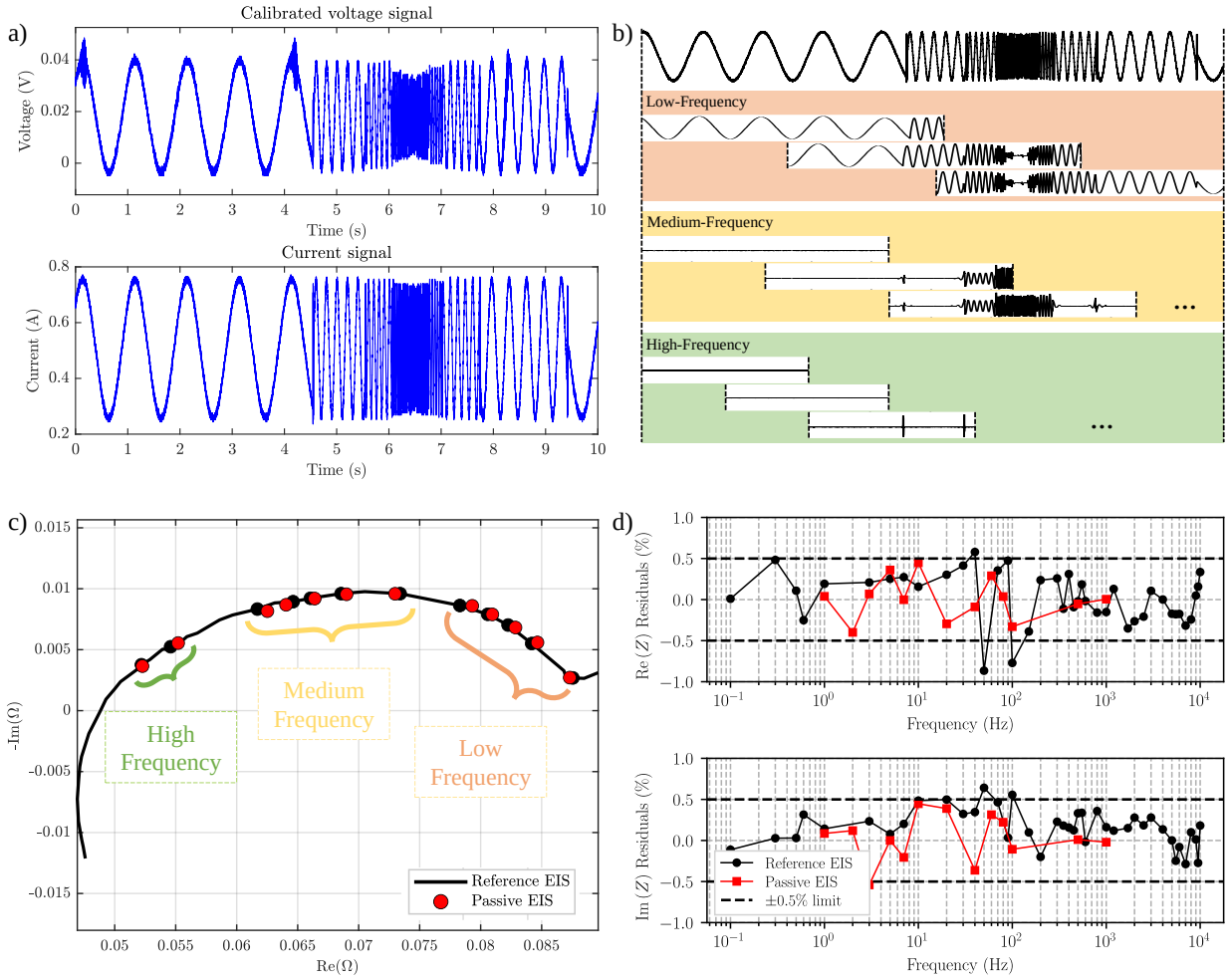


Figure 6: (a) Raw measured current and voltage signals, (b) Current after filtering and segmenting for the three frequency ranges, (c) Impedance calculated by DFT for each segment, averaged over 10 seconds, (d) Error analysis using the Kramers-Kronig method

A strong correlation was identified between the curves and verified using the Kramers-Kronig method, confirming the linearity of the EIS measurements (Figure 6.d). This step validates the optimized algorithm under steady-state conditions, without prior knowledge of the injected frequencies, and over a duration of 10 seconds.

Table 5: Measured frequencies in each frequency range for passive EIS

| | **High frequencies** | **Medium frequencies** | **Low frequencies** |
|---|---|---|---|
| Measured frequencies (Hz) | 1000 500 | 100 80 60 40 20 | 10 7 5 3 1 |

Another aspect of the study focuses on evaluating the algorithm's ability to detect superimposed excitation signals with different amplitudes. So far, the frequencies were injected sequentially, which does not necessarily reflect the conditions encountered in embedded systems. A multi-sine excitation was therefore implemented, allowing several frequencies with

different amplitudes to be superimposed simultaneously. The cycle presented in the table below was tested and analyzed using passive EIS (Table 6).

Table 6: Reference EIS vs Passive EIS - Amplitude

| **Process** | **Reference EIS** | **Passive EIS - Amplitude** |
|---|---|---|
| Current | 0.5A | 0.5A |
| Sinus injection | 0.1 Hz to 10 kHz | Multi-sine varying from 1 Hz to 1 kHz |
| Sinus amplitude | C/10 | Varies between C/30 and C/10 |
| Sampling frequency | 250 Hz to 25 MHz | 10 kHz |
| EIS duration | 3 min 30 | 8 seconds |
| Outside temperature | 25°C | 25°C |
| SoC | ≈ 100% | ≈ 100% |
| Signal processing algorithm | Conventional | Optimized |

As shown in Figure 7.a, the measured signal is significantly different from what has been observed so far. However, when comparing the reference impedance spectrum with the estimated impedance points (Figure 7.b), a very good correlation is observed.

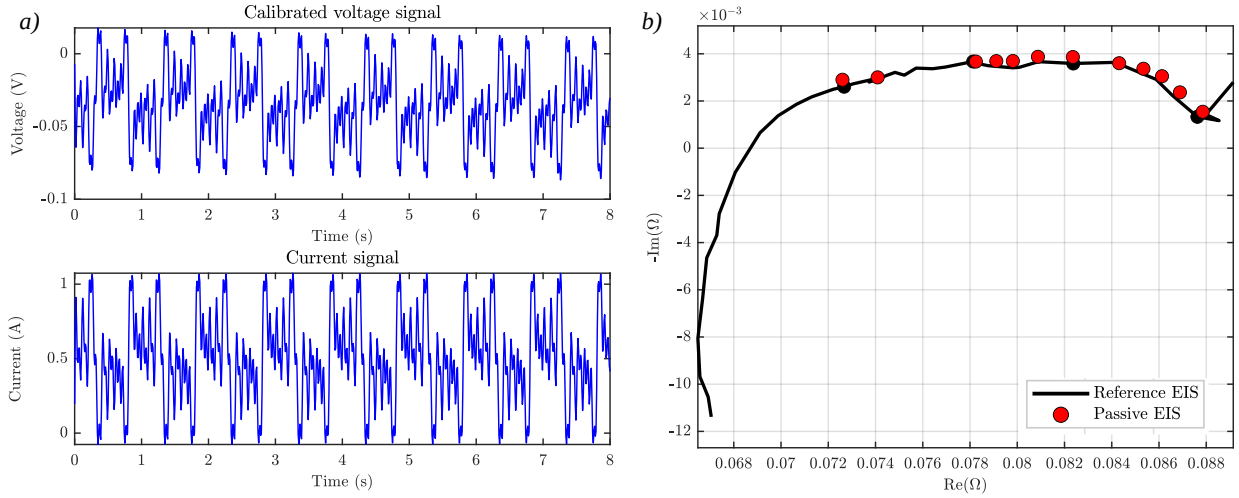


Figure 7: (a) Raw measured current and voltage signals with multi-sine injection, (b) Impedance calculated using the DFT for each segment, averaged over 8 seconds

It is nonetheless important to note that the system studied in this work is only weakly current-dependent. In systems where this dependence is stronger, certain precautions should be taken. Indeed, the amplitudes present in the system can affect the accuracy of impedance measurements: if they are too high, measurements may be distorted due to nonlinearity. It is also important to note that identifying harmonics with different amplitudes implies that if the amplitude is too low, the algorithm may not detect them. Real cycles were analyzed, and it was found that high-amplitude harmonics are rare. However, if they do occur, the averaging process helps to smooth out the impedance values. Additionally, one approach not

directly implemented in the algorithm is to use the Kramer-Kronig equations to check for linearity, which would allow the removal of nonlinear segments.

The two experiments conducted make it possible to move on to the next stage: calculating impedance under dynamic, non-stationary conditions.

## 4.5 Monitoring of Impedance Z=f(T) over a Driving Cycle

The objective of this section is to validate the concept of passive EIS under dynamic conditions. To do so, a driving cycle is injected, supplemented with several harmonics representing the system's natural components, all under varying temperature and SoC conditions. The goal is to use the optimized signal processing algorithm to passively calculate the impedance, then compare the results with the previously established reference EIS from the mapping, utilizing surface temperature measurements and SoC estimation.

### 4.5.1 Driving Cycle and Algorithm Parameterization

The cell is subjected to a 40-minute profile designed to induce dynamic variations in current, SoC, and temperature (Figure 8.a). This profile is tailored to the cell's technical specifications, including its nominal current and capacity.

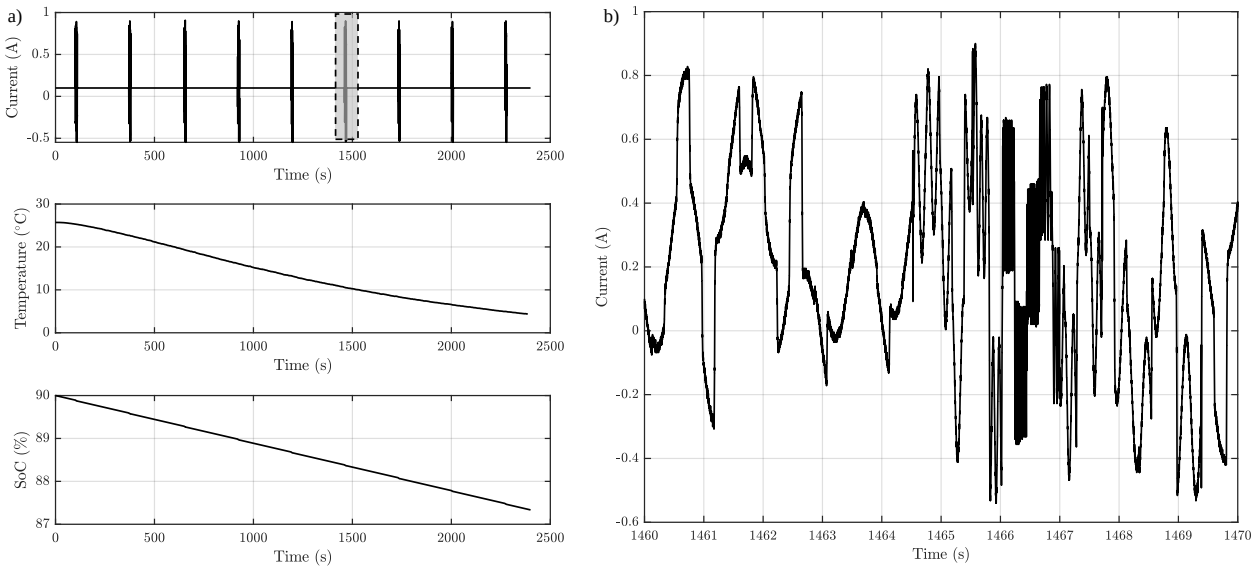


Figure 8: (a) Dynamic profile of current, state of charge, and temperature; (b) Zoomed-in view of a 10-second segment

The goal is to demonstrate the method's ability to detect and track variations in cell impedance. To do this, a test reproduces impedance changes related to SoC, temperature, or

current. These variations are monitored at regular intervals using passive EIS. The chosen interval corresponds to the resolution needed to observe impedance changes that are significant in relation to SoC and temperature.

Thus, every 4 minutes, an impedance measurement is taken over 10 seconds. This measurement, based on passive EIS, relies on a driving sequence constructed from the harmonics present in a representative driving cycle (Figure 8.b). In an onboard application, the passive EIS process would be applied continuously.

During impedance measurements, the signal is sampled at a frequency of 10 kHz, allowing the detection of present frequencies with a sufficient number of points. Harmonic content in the system is generated by the Chroma. In this case, their amplitude follows the references presented in section 3.1, where the natural harmonic content of the system was identified through EIS.

As for the mean value, setting the current to 0.1 A without harmonics between dynamic cycles was a deliberate choice, since no measurement is taken during that period. This part isn't meant to reflect actual behavior, but it's needed to simulate the cell discharge.

This entire current profile was reproduced using the test bench, which allows faithful injection of the desired signal. The objective is therefore to identify, via the signal processing algorithm, the impedances under dynamic conditions using a passive approach, without prior knowledge of the frequency content. During the studied cycle, the cell experiences a temperature variation from 25°C to 5°C according to the protocol detailed in Table 7.

Table 7: Dynamic condition test protocol

| | **Process** | **Units** |
|---|---|---|
| 1 | Set the Temperature of the cell in the thermal Chamber | 30 min before test at 25°C |
| 2 | Measure OCV, Calculate SoC | Instantaneous before Test |
| 3 | Cell preheating | 2 min at 0.25C and 2 min at -0.25C |
| 4 | Set the Temperature of the cell in the thermal Chamber | 5°C, dynamic condition |
| 5 | Injected driving cycle | 10 sec, 10 kHz |
| 6 | Discharge cell | 0.1 A, 0.05C for 250 s |
| 7 | Repeat (steps 5, 6 until temperature drops to 5°C) | |

The impedance measurement relies on the proper parameterization of the signal processing algorithm. As previously presented, the optimal parameters were selected (Table 8). The current and voltage of the cycle were measured, along with the associated surface temperature. Then, using Coulomb counting, an estimation of the SoC throughout the cycle was performed. For simplicity, the cell's internal temperature is here assumed to be equal to its surface temperature.

Table 8: Signal processing algorithm parameters

| Parameter | High frequencies | Medium frequencies | Low frequencies |
|---|---|---|---|
| Signal duration | | 2400 sec | |
| Sampling frequency before decimation | | 10 kHz | |
| Windowing | | Hamming | |
| Number of points per segment | | 100 | |
| Decimation | 1 | 10 | 100 |
| Overlap | 50% | 80% | 90% |
| Cutoff frequency of the anti-aliasing filter | 1250 Hz | 200 Hz | 50 Hz |
| Cutoff frequency of the low-pass filter | 75 Hz | 10 Hz | 0.5 Hz |

### 4.5.2 Measured Impedances

The output of the signal processing algorithm is displayed on a 3D Nyquist plot that incorporates the time dimension. This allows visualization of the impedance evolution over time, reflecting its variation during the temperature dynamics. The algorithm is calibrated to identify and average impedances over 10-second intervals, thus generating as many spectra as there are 10-second cycles injected, in this case, nine. Importantly, the algorithm processes the signals without prior knowledge of their frequency content.

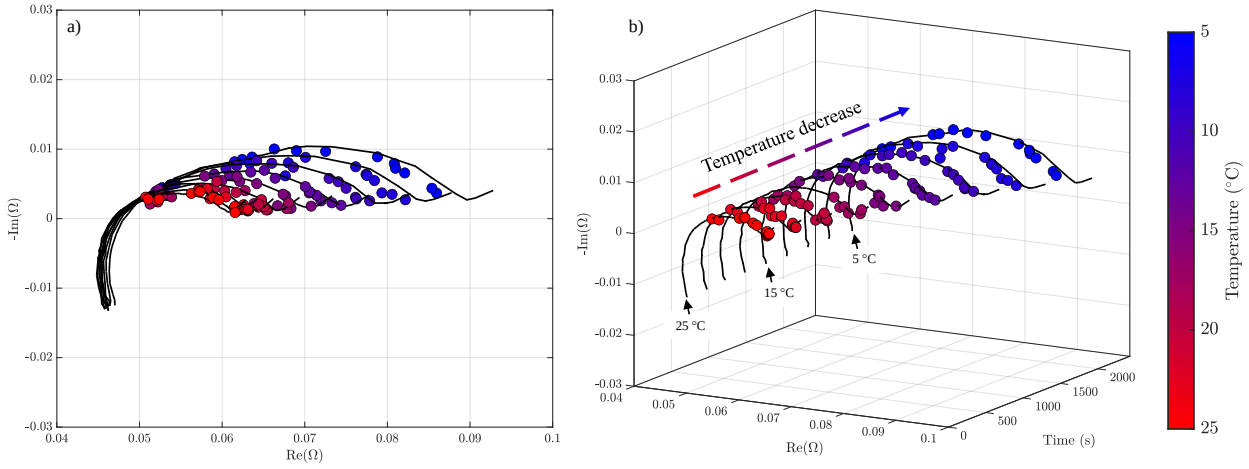


Figure 9: (a) Evolution of impedance on a 2D Nyquist plot. (b) Impedance monitoring over 40 minutes under dynamic conditions

To validate the passive impedance measurement, the obtained spectra are compared with reference EIS measurements. As shown earlier, spectra were recorded at different temperatures, which makes it possible to know the impedance at each temperature. During the driving cycle, the surface temperature is continuously monitored to track its evolution, and the SoC is recorded the same way. By combining the surface temperature and the SoC, each impedance measurement from the cycle can be matched to the corresponding reference spectra.

The Figure 9.a illustrates this: the raw reference spectra are shown in black, and the impedances measured during the cycle appear in red.

The passive impedance method correlates well with the reference EIS (Figure 9). A small discrepancy is observed between the passive EIS and the reference EIS due to temperature. Indeed, even a slight variation in temperature can have a significant impact on the impedance. A more accurate measurement of the cell temperature, particularly regarding the estimation of the internal temperature, could reduce this error. Table 9 shows the relative errors for three frequencies at three different temperatures. The maximum error is around 3%, indicating a fairly good agreement between the two EIS measurements.

Table 9: Relative error calculated for 3 frequencies at 3 different temperatures

| Temperature | Reference EIS | Passive EIS | Rel. Error |
|---|---|---|---|
| 1000 Hz | | | |
| 25°C | 0.0495+0.0021i | 0.0511+0.0028i | 3.29% |
| 15°C | 0.0497+0.0028i | 0.0514+0.0032i | 3.46% |
| 5°C | 0.0514+0.0037i | 0.0527+0.0045i | 2.64% |
| 20 Hz | | | |
| 25°C | 0.0596+0.0024i | 0.0596+0.0027i | 0.02% |
| 15°C | 0.0647+0.005i | 0.0642+0.005i | 0.77% |
| 5°C | 0.0733+0.0103i | 0.0725+0.0097i | 1.18% |
| 1 Hz | | | |
| 25°C | 0.0609+0.009i | 0.0617+0.0013i | 1.33% |
| 15°C | 0.07+0.0017i | 0.0708+0.0018i | 1.15% |
| 5°C | 0.0884+0.0035i | 0.086+0.0037i | 2.7% |

This also demonstrates the relevance of the proposed passive approach, which can detect both high and low frequencies under dynamic current, SoC, and temperature conditions. Such capability could enable monitoring of temperature or SoH through impedance measurements.

# 5 Conclusion

This article proposes a method to calculate the impedance of a Li-ion cell by exploiting the harmonic content naturally present in a driving cycle. Specifically:

- A preliminary study was conducted to identify these harmonics in signals from typical driving cycles.
- Based on this analysis, a signal processing algorithm was developed to calculate the impedance associated with these natural harmonics, regardless of their frequency and without prior knowledge of them. This introduces the concept of passive EIS, impedance spectroscopy performed without artificial excitation.
- One of the strengths of this algorithm lies in its ability to operate under dynamic conditions. This was made possible by integrating a drift compensation method designed to

separate effects related to signal non-stationarity from those genuinely due to battery excitation.

- The careful selection of algorithm parameters is essential to refine the accuracy of impedance measurement.

To validate the method, tests were conducted on a test bench by injecting a driving cycle with reconstructed harmonic content, subsequently analyzed using the optimized method. Then, based on SoC estimation and surface temperature measurement of the cell, a correlation between the reference EIS and the passive EIS was established, thereby validating the passively measured impedances.

This highlights the key advantage of the proposed method: using natural harmonics to monitor the cell's temperature or State of Health through impedance measurements. One of the future research directions will focus on developing a thermal model of the cell's internal temperature, with the aim of better capturing the influence of current on charge transfer and internal heating and further improving PEIS accuracy. Testing the method at the battery-pack level, using an equivalent impedance approach, would also bring it a step closer to real embedded applications.

# Acknowledgments

This work has been supported by the EIPHI Graduate school (contract "ANR-17-EURE-0002" and the Region of Bourgogne Franche-Comté).

The HYSySPEM project was funded by the “France 2030” government investment plan managed by the French National Research Agency, under the reference ANR-22-PEHY-0018.

# Declaration of Competing Interest

The authors declare that they have no known competing financial interests or personal relationships that could have appeared to influence the work reported in this paper.

# Data Availability Statement

The data that support the findings of this study were generated during the Hysyspem France 2030 project. These data are subject to confidentiality restrictions and are therefore

not publicly available. Data may be available from the corresponding author upon reasonable request and with permission of the project consortium.

## Author Contributions

**Conceptualization**: J. Millet, D. Depernet, A. Sari, F. Gustin, H. Helbling
**Methodology**: J. Millet, D. Depernet, A. Sari, F. Gustin, H. Helbling
**Investigation**: J. Millet
**Formal analysis**: J. Millet
**Writing – original draft**: J. Millet
**Writing – review & editing**: J. Millet, D. Depernet, A. Sari, F. Gustin, H. Helbling
**Supervision**: D. Depernet, A. Sari, F. Gustin, H. Helbling

## References


[1] Forum International des Transports. *Perspectives des transports FIT 2023*. en. Perspectives des transports FIT. OECD, Apr. 2024. ISBN: 978-92-821-1630-2 978-92-821-1507-7 978-92-821-1823-8. DOI: 10.1787/32bbcca5-fr.

[2] Osman Demirci et al. "Review of battery state estimation methods for electric vehicles-Part II: SOH estimation". en. In: *Journal of Energy Storage* 96 (Aug. 2024), p. 112703. ISSN: 2352152X. DOI: 10.1016/j.est.2024.112703.

[3] Wladislaw Waag, Christian Fleischer, and Dirk Uwe Sauer. "On-line estimation of lithium-ion battery impedance parameters using a novel varied-parameters approach". en. In: *Journal of Power Sources* 237 (Sept. 2013), pp. 260–269. ISSN: 03787753. DOI: 10.1016/j.jpowsour.2013.03.034.

[4] Christian Fleischer et al. "On-line adaptive battery impedance parameter and state estimation considering physical principles in reduced order equivalent circuit battery models". en. In: *Journal of Power Sources* 260 (Aug. 2014), pp. 276–291. ISSN: 03787753. DOI: 10.1016/j.jpowsour.2014.01.129.

[5] Sijia Yang et al. "Review on state-of-health of lithium-ion batteries: Characterizations, estimations and applications". en. In: *Journal of Cleaner Production* 314 (Sept. 2021), p. 128015. ISSN: 09596526. DOI: 10.1016/j.jclepro.2021.128015.

[6] Xinghao Du et al. “Feature selection strategy optimization for lithium-ion battery state of health estimation under impedance uncertainties”. en. In: *Journal of Energy Chemistry* 101 (Feb. 2025), pp. 87–98. ISSN: 20954956. DOI: 10.1016/j.jechem.2024.09.032.

[7] Charles Bechara et al. “Estimation of the Internal Temperature of High-Capacity Li-Ion Cells Using Embedded Impedancemetry”. en. In: *IEEE Open Journal of Vehicular Technology* 6 (2025). Publisher: Institute of Electrical and Electronics Engineers (IEEE), pp. 1686–1697. ISSN: 2644-1330. DOI: 10.1109/ojvt.2025.3579059.

[8] Sudnya Vaidya et al. “State of temperature detection of Li-ion batteries by intelligent gray box model”. en. In: *Journal of Power Sources* 585 (Nov. 2023), p. 233624. ISSN: 03787753. DOI: 10.1016/j.jpowsour.2023.233624.

[9] Daniel Depernet, Oumar Ba, and Alain Berthon. “Online impedance spectroscopy of lead acid batteries for storage management of a standalone power plant”. en. In: *Journal of Power Sources* 219 (Dec. 2012), pp. 65–74. ISSN: 03787753. DOI: 10.1016/j.jpowsour.2012.07.053.

[10] Hamzeh Beiranvand et al. “Review of Power Converter Topologies for Electrochemical Impedance Spectroscopy of Lithium-Ion Batteries”. en. In: ().

[11] Erfan Sadeghi et al. “Controllable Electrochemical Impedance Spectroscopy: From Circuit Design to Control and Data Analysis”. en. In: *IEEE Transactions on Power Electronics* 35.9 (Sept. 2020), pp. 9933–9942. ISSN: 0885-8993, 1941-0107. DOI: 10.1109/TPEL.2020.2977274.

[12] Bernhard Liebhart, Lidiya Komsiyska, and Christian Endisch. “Passive impedance spectroscopy for monitoring lithium-ion battery cells during vehicle operation”. en. In: *Journal of Power Sources* 449 (Feb. 2020), p. 227297. ISSN: 03787753. DOI: 10.1016/j.jpowsour.2019.227297.

[13] Nils Lohmann et al. “Employing Real Automotive Driving Data for Electrochemical Impedance Spectroscopy on Lithium-Ion Cells”. en. In: *SAE International Journal of Alternative Powertrains* 4.2 (Apr. 2015), pp. 308–317. ISSN: 2167-4205. DOI: 10.4271/2015-01-1187.

[14] Bowen Yang et al. “Research on online passive electrochemical impedance spectroscopy and its outlook in battery management”. en. In: *Applied Energy* 363 (June 2024), p. 123046. ISSN: 03062619. DOI: 10.1016/j.apenergy.2024.123046.

[15] C. A. Schiller et al. “Validation and evaluation of electrochemical impedance spectra of systems with states that change with time”. en. In: *Physical Chemistry Chemical Physics* 3.3 (2001), pp. 374–378. ISSN: 14639076, 14639084. DOI: 10.1039/b007678n.

[16] Alexandros Ch. Lazanas and Mamas I. Prodromidis. “Electrochemical Impedance SpectroscopyA Tutorial”. en. In: *ACS Measurement Science Au* 3.3 (June 2023), pp. 162–193. ISSN: 2694-250X, 2694-250X. DOI: 10.1021/acsmeasuresciau.2c00070.

[17] Markos Koseoglou et al. “Lithium plating detection using dynamic electrochemical impedance spectroscopy in lithium-ion batteries”. en. In: *Journal of Power Sources* 512 (Nov. 2021), p. 230508. ISSN: 03787753. DOI: 10.1016/j.jpowsour.2021.230508.

[18] Sara Drvarič Talian et al. “Impedance spectroscopy applied to lithium battery materials: Good practices in measurements and analyses”. en. In: *Energy Storage Materials* 69 (May 2024), p. 103413. ISSN: 24058297. DOI: 10.1016/j.ensm.2024.103413.

[19] Xinghao Du et al. “Exploring impedance spectrum for lithium-ion batteries diagnosis and prognosis: A comprehensive review”. en. In: *Journal of Energy Chemistry* 95 (Aug. 2024), pp. 464–483. ISSN: 20954956. DOI: 10.1016/j.jechem.2024.04.005.

[20] Jiahua Li et al. “Internal temperature estimation method for lithium-ion battery based on multi-frequency imaginary part impedance and GPR model”. en. In: *Journal of Energy Storage* 118 (May 2025), p. 116287. ISSN: 2352152X. DOI: 10.1016/j.est.2025.116287.

[21] Noël Hallemans et al. “Electrochemical impedance spectroscopy beyond linearity and stationarity—A critical review”. en. In: *Electrochimica Acta* 466 (Oct. 2023). Publisher: Elsevier BV, p. 142939. ISSN: 0013-4686. DOI: 10.1016/j.electacta.2023.142939.

[22] Cheng Guo et al. “Review of the calculation of DC-link capacitor current”. en. In: *Frontiers in Energy Research* 11 (Aug. 2023), p. 1240755. ISSN: 2296-598X. DOI: 10.3389/fenrg.2023.1240755.

[23] B.P. McGrath and D.G. Holmes. “A General Analytical Method for Calculating Inverter DC-Link Current Harmonics”. en. In: *IEEE Transactions on Industry Applications* 45.5 (2009), pp. 1851–1859. ISSN: 0093-9994, 1939-9367. DOI: 10.1109/TIA.2009.2027556.

[24] Jianjun Hu et al. “Research on Harmonic Torque Reduction Strategy for Integrated Electric Drive System in Pure Electric Vehicle”. en. In: *Electronics* 9.8 (Aug. 2020), p. 1241. ISSN: 2079-9292. DOI: 10.3390/electronics9081241.

[25] Gerald Goertzel. “An Algorithm for the Evaluation of Finite Trigonometric Series”. en. In: *The American Mathematical Monthly* 65.1 (Jan. 1958), p. 34. ISSN: 00029890. DOI: 10.2307/2310304.

[26] F.J Owens and M.S Murphy. “A short-time Fourier transform”. en. In: *Signal Processing* 14.1 (Jan. 1988), pp. 3–10. ISSN: 01651684. DOI: 10.1016/0165-1684(88)90040-0.

[27] Jérôme Antoni and Johan Schoukens. “A comprehensive study of the bias and variance of frequency-response-function measurements: Optimal window selection and overlapping strategies”. en. In: *Automatica* 43.10 (Oct. 2007), pp. 1723–1736. ISSN: 00051098. DOI: 10.1016/j.automatica.2007.02.020.

[28] Slater Twain Bakenhaster and Howard D. Dewald. “Electrochemical impedance spectroscopy and battery systems: past work, current research, and future opportunities”. en. In: *Journal of Applied Electrochemistry* 55.7 (July 2025). Publisher: Springer Science and Business Media LLC, pp. 1657–1681. ISSN: 0021-891X, 1572-8838. DOI: 10.1007/s10800-025-02273-6.

[29] Laura Bravo Diaz. “Measuring Irreversible Heat Generation in Lithium-Ion Batteries: An Experimental Methodology”. en. In: *Journal of The Electrochemical Society* (2022).

[30] Wenlin Zhang, Ryan Ahmed, and Saeid Habibi. “Understanding the impact of recent usage on lithium-ion battery impedance through the relaxation phenomena”. en. In: *Journal of Power Sources* 630 (Feb. 2025), p. 236108. ISSN: 03787753. DOI: 10.1016/j.jpowsour.2024.236108.

[31] D. Andre et al. “Characterization of high-power lithium-ion batteries by electrochemical impedance spectroscopy. I. Experimental investigation”. en. In: *Journal of Power Sources* 196.12 (June 2011), pp. 5334–5341. ISSN: 03787753. DOI: 10.1016/j.jpowsour.2010.12.102.

[32] Jiangong Zhu et al. “Studies on the medium-frequency impedance arc for Lithium-ion batteries considering various alternating current amplitudes”. en. In: *Journal of Applied Electrochemistry* 46.2 (Feb. 2016). Publisher: Springer Science and Business Media LLC, pp. 157–167. ISSN: 0021-891X, 1572-8838. DOI: 10.1007/s10800-015-0887-z.

[33] Zheyuan Pang et al. “A new method for determining SOH of lithium batteries using the real-part ratio of EIS specific frequency impedance”. en. In: *Journal of Energy Storage* 72 (Nov. 2023), p. 108693. ISSN: 2352152X. DOI: 10.1016/j.est.2023.108693.

[34] M. Schönleber, D. Klotz, and E. Ivers-Tiffée. "A Method for Improving the Robustness of linear Kramers-Kronig Validity Tests". en. In: *Electrochimica Acta* 131 (June 2014), pp. 20–27. ISSN: 00134686. DOI: 10.1016/j.electacta.2014.01.034.

[35] Muhammad Sheraz and Woojin Choi. "A High-Speed Multichannel Electrochemical Impedance Spectroscopy System Using Broadband Multi-Sine Binary Perturbation for Retired Li-Ion Batteries of Electric Vehicles". en. In: *Energies* 17.12 (June 2024). Publisher: MDPI AG, p. 2979. ISSN: 1996-1073. DOI: 10.3390/en17122979.